Earth and Planetary Science Letters 546 (2020) 116444

Contents lists available at ScienceDirect

Earth and Planetary Science Letters

www.elsevier.com/locate/epsl

Isotopic and textural analysis of giant unmelted micrometeorites – identification of new material from intensely altered ^{16}O-poor water-rich asteroids

M.D. Suttle [a,b,*], Z. Dionnet [c,d], I. Franchi [e], L. Folco [a,f], J. Gibson [e], R.C. Greenwood [e], A. Rotundi [c], A. King [g], S.S. Russell [b]

[a] Dipartimento di Scienze della Terra, Università di Pisa, Via S. Maria 53, 56126 Pisa, Italy
[b] Planetary Materials Group, Department of Earth Sciences, Natural History Museum, Cromwell Road, London, SW7 5BD, UK
[c] DIST-Università di Napoli "Parthenope", Centro Direzionale Isola C4, 80143 Naples, Italy
[d] INAF-IAPS, via Fosso del Cavaliere 100, 00133 Rome, Italy
[e] School of Physical Sciences, The Open University, Walton Hall, Milton Keynes, MK7 6AA, UK
[f] CISUP, Centro per l'Integrazione della Strumentazione dell'Università di Pisa, Lungarno Pacinotti 43, 56126 Pisa, Italy
[g] Psiche beamline, Synchrotron SOLEIL, Orne des Meurisiers, France

ARTICLE INFO

Article history:
Received 12 April 2020
Received in revised form 25 June 2020
Accepted 26 June 2020
Available online 13 July 2020
Editor: W.B. McKinnon

Keywords:
micrometeorites
carbonaceous chondrites
O-isotopes
water-to-rock ratio

ABSTRACT

Bulk oxygen isotope data has the potential to match extraterrestrial samples to parent body sources based on distinctive δ^{18}O and Δ^{17}O ratios. We analysed 10 giant (>500 μm) micrometeorites using combined micro-Computer Tomography (μCT) and O-isotope analysis to pair internal textures to inferred parent body groups. We identify three ordinary chondrite particles (L and LL groups), four from CR chondrites and the first micrometeorite from the enstatite chondrite (EH4) group. In addition, two micrometeorites are from hydrated carbonaceous chondrite parent bodies with ^{16}O-poor isotopic compositions and plot above the terrestrial fractionation line. They experienced intense aqueous alteration, contain pseudomorphic chondrules and are petrographically similar to the CM1/CR1 chondrites. These micrometeorites may be members of the newly established CY chondrites and/or derived from the enigmatic "*Group 4*" micrometeorite population, previously identified by Yada et al., 2005 [GCA, 69:5789-5804], Suavet et al., 2010 [EPSL, 293:313-320] (and others). One of our ^{16}O-poor micrometeorite plots on the same isotopic trendline as the CO, CM and CY chondrites – "*the CM mixing line*" (with a slope of ~0.7 and a δ^{17}O intercept of -4.23‰), this implies a close relationship and potentially a genetic link to these hydrated chondrites. If position along the CM mixing line reflects the amount of ^{16}O-poor (heavy) water-ice accreted onto the parent body at formation, then the CY chondrites and these ^{16}O-poor micrometeorites must have accreted at least as much water-ice as CM chondrites but potentially more. In addition, thermal metamorphism could have played a role in further raising the bulk O-isotope compositions through the preferential loss of isotopically light water during phyllosilicate dehydration. The study of micrometeorites provides insights into asteroid belt diversity through the discovery of material not currently sampled by larger meteorites, perhaps as a result of atmospheric entry biases preventing the survival of large blocks of friable hydrated material.

1. Introduction

Micrometeorites are millimetre-sized dust grains which originate from solar system small bodies (Genge et al., 2008; Folco and Cordier, 2015). Their analysis provides information on the composition of asteroids and comets (Gounelle et al., 2009; Cordier and Folco, 2014) and helps us to better understand the origin and evolution of the protoplanetary disk. Furthermore, data from micrometeorites provide a complementary perspective to the insights

* Corresponding author at: Dipartimento di Scienze della Terra, Università di Pisa, Via S. Maria 53, 56126 Pisa, Italy.
E-mail addresses: martindavid.suttle@dst.unipi.it (M.D. Suttle), zelia.dionnet@uniparthenope.it (Z. Dionnet), ian.franchi@open.ac.uk (I. Franchi), luigi.folco@unipi.it (L. Folco), jennifer.gibson@open.ac.uk (J. Gibson), r.c.greenwood@open.ac.uk (R.C. Greenwood), alessandra.rotundi@inaf.it (A. Rotundi), king@synchrotron-soleil.fr (A. King), sara.russell@nhm.ac.uk (S.S. Russell).

https://doi.org/10.1016/j.epsl.2020.116444
0012-821X/

obtained from the study of larger meteorites and from space mission sample returns (e.g. STARDUST, OSIRIS-REx and HAYABUSA [I & II]).

The composition of the micrometeorite flux reaching Earth today is dominated by hydrated carbonaceous chondrites with affinities to the CM, CR and CI chondrites (Taylor et al., 2012). In addition, some particles resemble the ungrouped meteorite Tagish Lake (Sakamoto et al., 2010). Fine-grained micrometeorites represent ≫50% of unmelted micrometeorites across all size fractions (Taylor et al., 2012) and are therefore a major component of the near-Earth dust complex (Cordier and Folco, 2014). Conversely, coarse-grained micrometeorites which are primarily chondrule and CAI (Ca-, Al-rich inclusions) fragments (Genge et al., 2005) represent a smaller component of the micrometeorite flux (<25%, Prasad et al., 2018).

Resolving the parent body affinities of hydrated fine-grained micrometeorites is particularly difficult because they share similar petrology, which can be significantly overprinted by later atmospheric entry and terrestrial weathering effects (Suttle et al., 2019a). This has led to a number of studies with contradictory conclusions. Specifically, it remains unclear whether fine-grained micrometeorites sample the same asteroids as established chondrite groups or whether micrometeorites also include contributions from parent bodies otherwise unsampled by meteorite collections.

Engrand and Maurette (1998) concluded that micrometeorites are primarily derived from "*a new population of solar system objects, probably formed in the outer solar system*" whose parent bodies are "*chondrites-without-chondrules*". Later, Sakamoto et al. (2010) suggested the presence of serpentine/saponite intergrowths, combined with Mg-carbonate and lacking anhydrous silicates represented a new population of micrometeorites. Battandier et al. (2018) echoed similar conclusions, suggesting that micrometeorites "*originate from* [. . .] *distinct parent bodies with respect to primitive carbonaceous chondrites* [which are characterised by] *higher* CH_2/CH_3 *ratio* [s] *and a smaller carbonyl abundance than chondrites*". In contrast, other studies have identified individual particles with direct links to CM, CR and CI chondrites (Genge et al., 2005; van Ginneken et al., 2012). Likewise, we previously suggested that the micrometeorite flux should logically include both contributions from established chondrite groups as well as otherwise unsampled parent bodies (Suttle et al., 2019a).

To better constrain the relative proportions of fine-grained micrometeorites derived from known and new parent bodies requires a multi-analytical approach. To gain the maximum amount of information from each particle we pair particle micro-textures obtained using high-resolution synchrotron micro-Computer Tomography (μCT) with bulk triple oxygen isotope measurements – thereby linking particle texture to parentage with reduced ambiguity. Our study has several advantages over previous O-isotope work on micrometeorites:

(1) Only unmelted and partially melted micrometeorites (termed scoriaceous and defined as having experienced <50% melting [Genge et al., 2008]) were used in this study. These are significantly less affected by mass-dependent fractionation overprints inherited during atmospheric entry as compared to the completely melted cosmic spherules. Consequently, the isotope compositions of unmelted and scoriaceous micrometeorites plot closer to their true parent body signatures (Cordier and Folco, 2014), rather than shifted to higher $\delta^{18}O$ values as is the case for cosmic spherules (e.g. Suavet et al., 2010; van Ginneken et al., 2017). Likewise, unmelted and scoriaceous micrometeorites should exhibit less isotopic contamination arising from oxygen exchange with Earth's atmosphere; both related processes are referred to here as isotopic [atmospheric] entry effects.

(2) In addition, this study avoided particles with clear evidence of terrestrial weathering (section 2). This is important because interaction with terrestrial water can alter the O-isotopic composition of extraterrestrial materials, shifting their compositions towards isotopically light terrestrial values (Alexander et al., 2018).

(3) Finally, the use of laser fluorination mass spectrometry provides higher precision data (see details in section 2 below) and proportionally lower error, as compared to ion-probe and nanoSIMS measurements [±1.2-3.2‰ for $\delta^{18}O$ (2σ) and ±0.6-1.7‰ for $\Delta^{17}O$ (2σ), as seen in Engrand et al. (2005); Yada et al. (2005); Gounelle et al. (2005)]. This ensures higher confidence in parent body designations and may potentially allow the classification of micrometeorites to specific chondrite types (e.g. identifying LL or L chondrites rather than simply ordinary chondrites).

2. Materials and methods

2.1. Samples (main population)

Micrometeorites studied here are derived from the Transantarctic Mountains (TAM) micrometeorite collection. They were recovered from loose subaerial sediments, accumulated within joints and weathering pits on flat glacially eroded summit plateaus exposed above the local ice sheet over the last ∼1 million years (Rochette et al., 2008). The accumulation and terrestrial evolution of this collection is uniquely well-characterised (van Ginneken et al., 2016; Suttle and Folco, 2020). Due to the long accumulation time, particles tend to be variably altered by terrestrial weathering, which results in the progressive replacement of primary micrometeorite phases with secondary jarosite, calcite, palagonite, and ferrihydrite (van Ginneken et al., 2016). However, the TAM collection also contains an abundance of large micrometeorites which are otherwise exceptionally rare or absent among other collections. The advantage of studying giant (>500 μm) micrometeorites lies in the ability to analyse a more representative sample of their parent body. Likewise, larger particles allow a wider range of micro-analytical techniques on individual particles, including bulk laser fluorination O-isotope mass spectrometry, as performed here.

The giant micrometeorites analysed in this study were primarily recovered from rock traps (TAM50; 72°42.068' S, 160°14.303' E) on Miller Butte in Victoria Land, Antarctica (Suavet et al., 2009) during the 2012-13 Programma Nazionale delle Ricerche in Antartide (PNRA) expedition. Picked particles were photographed under binocular microscope and their exteriors were analysed using SEM-BSE imaging using a FEI Quanta 450 ESEM-FEG equipped with EDS Bruker, QUANTAX XFlash Detector 6|10 at the Centro per l'Integrazione della Strumentazione dell'Università di Pisa (CISUP), Italy. This initial characterisation allowed their degree of terrestrial weathering and degree of atmospheric entry heating to be estimated based on particle shape and exterior surface textures. Unmelted micrometeorites have irregular shapes while scoriaceous micrometeorites have rounded shapes with smooth surfaces (Genge et al., 2008; Folco and Cordier, 2015). The degree of weathering can be inferred based on the presence and thickness of encrustation rims. These are commonly composed of jarosite, halite and/or Fe-oxyhydroxides (van Ginneken et al., 2016). Encrustation rims appear dark (low Z contrast) in BSE images and are therefore resolvable from the micrometeorite's surface which otherwise appears bright (high Z contrast). This is because all micrometeorites develop a thin covering of magnetite on their surface during atmospheric entry. This is termed magnetite rim and is often used as diagnostic criteria for the identification of micrometeorites and to distinguish micrometeorites from meteorite fragments or ablation debris (Genge et al., 2008).

We selected a subset of 26 micrometeorites for further analysis, using the criteria of large size (>500 μm), minimal evidence of terrestrial weathering and low degree of flash melting – our selection included both fine-grained and coarse-grained representatives.

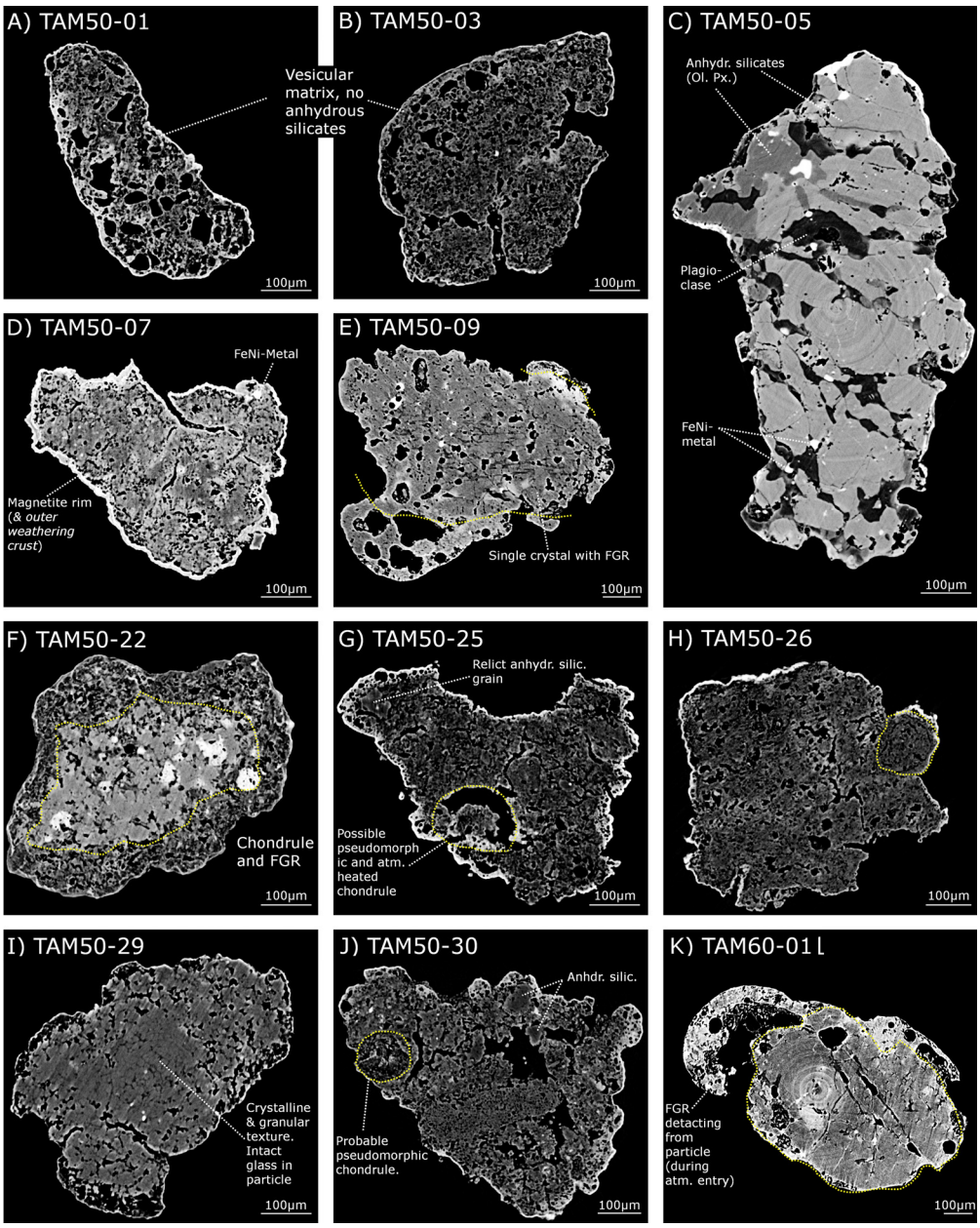

Fig. 1. Image panel showing µCT slices through eleven of the TAM particles investigated in this study (the remaining particle textures can be seen in Fig. 2 and Fig. 3). Annotations provide interpretation of sample mineralogy and textures. Dashed yellow lines mark interpreted boundaries of chondrules or former chondrules (now observed as chondrule pseudomorphs). (For interpretation of the colours in the figure(s), the reader is referred to the web version of this article.)

2.2. Experimental

Each micrometeorite particle was analysed further using synchrotron µCT, collected on the PSICHE beamline of the SOLEIL synchrotron (Paris, France). Micro-CT measurements used a monochromatic beam, operating at 25 keV. In total, 1200 tomographic slices were collected on each particle with an exposure time of 0.25 s per projection and a rotation rate of 0.15° per projection. The final 3D models have a resolution of ~0.66 µm voxel size. The raw reconstructed scans were filtered using a nonlocal means edge preserving filter, which reduced image noise arising from beam attenuation, hardening and ring artefacts (Figs. 1, 2 & 3).

Following non-destructive pre-characterisation, the triple oxygen isotope composition of 14 particles was determined at the Open University in Milton Keynes, UK, using infrared laser-assisted fluorination mass spectrometry (Miller et al., 1999; Greenwood et al., 2017). Prior to analysis, micrometeorites were weighed and treated with acetone to remove residual organic contamination, potentially arising from their (scotch tape) mounting used in the pre-characterisation phase. We then treated the particles with EATG (ethanolamine thioglycolate). This partially removes terrestrial isotopic contamination effects resulting from the presence of secondary Fe-bearing minerals formed during weathering (Greenwood et al., 2017).

The Open University laser fluorination system operates by reacting each sample in turn with an aliquot of BrF_5 gas. Rapid reaction with BrF_5 takes place by heating the sample using an IR laser (Miller et al., 1999; Greenwood et al., 2017). The BrF_5 reaction liberates chemically bound oxygen within the sample, which is then purified by passing it through two cryogenic nitrogen traps, separated by a bed of heated KBr. This latter stage removes residual (unreacted) F_2 gas by forming KF. The Br_2 released by this reaction is frozen down in the second nitrogen trap. The purified oxygen gas is then collected onto a cryogenic trap containing 13X

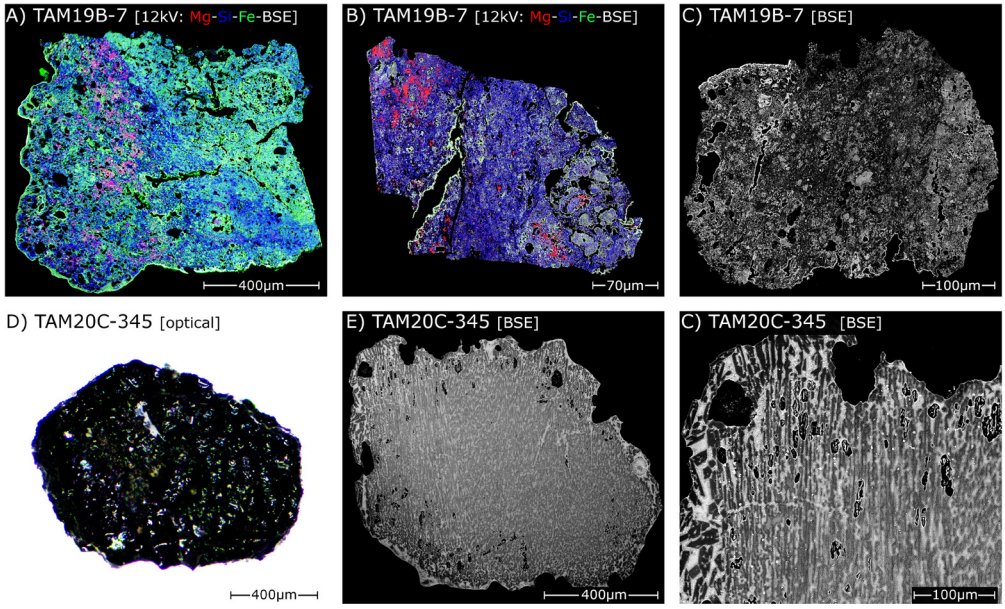

Fig. 2. SEM-BSE images of TAM19B-7 (A-C) and TAM20C-345 (D-F). TAM19B-7 is the largest unmelted fine-grained micrometeorite discovered. Its internal texture, observed in three sections, reveals an intensely aqueously altered and highly weathered history. This micrometeorite contains numerous pseudomorphic chondrules and no anhydrous silicates. In contrast TAM20C-345 is a fresh (unweathered) coarse-grained micrometeorite composed of euhedral enstatite laths and minor Cr-spinels embedded within a Ca-rich glass. The particle has an outer rim with a coarser grain size and tiny vesicles, likely reflecting local partial melting (and subsequent recrystallisation) during atmospheric entry.

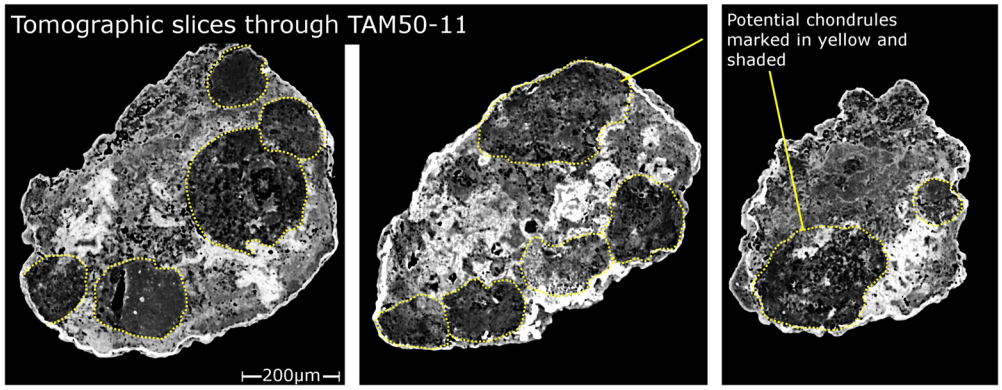

Fig. 3. Tomographic slices through TAM50-11. This particle is interpreted as an enstatite chondritic micrometeorite (EH4), based on the relatively high abundance of small (<250 μm) "*armoured*" chondrules (surrounded by high density phases, likely Fe-metal or Fe-sulfides) as well as the high abundance of Fe-rich phases and an O-isotopic signature consistent with this parent body group.

molecular sieve pellets. Following isolation from the rest of the clean-up line, the molecular sieve is then heated, and the trapped gas released into the inlet system of the mass spectrometer. With gas sample sizes greater than approximately 150 μg O_2 analysis is undertaken using conventional dual-inlet, gas source, isotope ratio mass spectrometry protocols (Miller et al., 1999; Greenwood et al., 2017). However, when measuring gas samples that are less than about 150 μg O_2 (typically sample masses <0.2 mg), there is insufficient gas to maintain laminar flow through the inlet capillaries and as consequence conventional dual-inlet analysis cannot be undertaken. When analysing such small samples, an extra trapping stage is required and the gas from the 13X molecular sieve is transferred to a cryogenic trap containing silica gel located within the inlet system of the MAT 253. On heating, the gas held on the silica gel trap is rapidly released into the inlet, without the use of the bellows system.

Oxygen isotopic analyses are reported here in standard δ notation, where $\delta^{18}O$ has been calculated as: $\delta^{18}O = [(^{18}O/^{16}O)_{sample}/(^{18}O/^{16}O)_{VSMOW} - 1]\ 1000$ (‰) and similarly for $\delta^{17}O$ using the $^{17}O/^{16}O$ ratio. $\Delta^{17}O$, which represents the deviation from the terrestrial fractionation has been calculated as $\Delta^{17}O = \delta^{17}O - 0.52\ \delta^{18}O$.

Laser fluorination is currently the highest precision method for measuring O-isotopic signatures whilst also being capable of analysing relatively small sample masses. Typically, 2 mg aliquots are taken from larger homogenised bulk samples (generally between 50 and 100 mg) and loaded along with various silicate standard materials (UWG-2 garnet, NBS-28 quartz, an internal obsidian standard). Repeat analysis (n = 38) of ~2 mg aliquots of the Open University internal obsidian standard gave the following results: 3.81 ± 0.05 ‰ for $\delta^{17}O$ (2σ); 7.27 ± 0.10 ‰ for $\delta^{18}O$ (2σ); 0.03 ± 0.02‰ for $\Delta^{17}O$ (2σ) (Starkey et al., 2016). When samples with masses lower than about 0.5 mg are analysed there is a systematic tendency towards lighter oxygen isotopic compositions and a decrease in precision. Both of these effects increase as sample size decreases. During the course of this and other recent micrometeorite studies undertaken at the Open University (Goderis et al., 2020), small obsidian samples were run in the same trays as

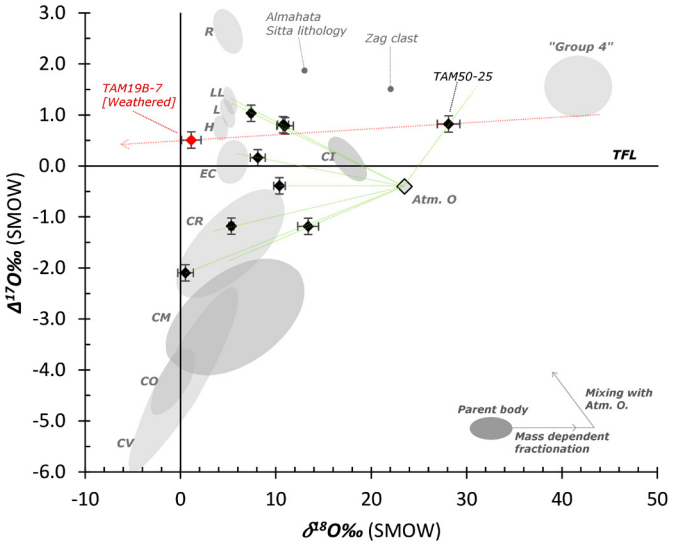

Fig. 4. TAM micrometeorites plotted in oxygen isotope space ($\delta^{18}O/\Delta^{17}O$). Green dashed lines show the assumed mixing between the micrometeorite's parent body and terrestrial atmospheric oxygen, while the dashed red line shows the assumed isotopic mixing between the parent body of TAM19B-7 and terrestrial Antarctic precipitation (SLAP has values: $\delta^{18}O \approx -50‰$, $\Delta^{17}O = 0‰$). The compositions of known chondrite groups are plotted as faded grey fields. The composition of the *Group 4* population as described by Suavet et al. (2010) of which TAM50-25 may be an (unmelted) member is also marked. Also labelled are the compositions of two anomalously heavy carbonaceous chondrite lithologies recently described from the Zag meteorite (Kebukawa et al., 2019) and the Almahata Sitta meteorite (Goodrich et al., 2019). The solid black line labelled "TFL" represents the terrestrial fractionation line ($\delta^{17}O = 0.52 \times \delta^{18}O$), while the grey diamond labelled "Atm. O" represents the average isotopic composition of Earth's mesospheric oxygen ($\delta^{17}O \approx 11.8‰$ and $\delta^{18}O \approx 23.5‰$, Thiemens et al., 1995). The inset in the bottom right graphically illustrates how the different atmospheric entry processes affect the parent body composition of a micrometeorite.

the micrometeorites to monitor both effects. Based on a compilation (n = 45) of these small obsidians (Fig. S1), it is apparent that samples with masses <0.1 mg are more significantly fractionated than those with masses >0.1 mg. Thus, obsidian samples (n = 27) in the mass range 0.10-0.26 mg gave the following average composition: 3.63 ± 0.48 ‰ for $\delta^{17}O$ (2σ); 6.97± 0.89 ‰ for $\delta^{18}O$ (2σ); 0.01 ± 0.05 ‰ for $\Delta^{17}O$ (2σ). In comparison, obsidians with a mass of <0.1 mg gave the following composition: 3.35 ± 0.58 ‰ for $\delta^{17}O$ (2σ); 6.47± 1.07 ‰ for $\delta^{18}O$ (2σ); -0.02 ± 0.05 ‰ for $\Delta^{17}O$ (2σ). However, micrometeorites display large isotopic differences (Table 1 Figs. 4 and 5) and consequently, the precision of the analyses obtained for even the smallest size fraction (<0.1 mg) is more than sufficient to fully characterise these materials.

2.3. Samples (other)

Two of the micrometeorites studied here (TAM19B-7 and TAM20C-345 [Fig. 2]) have different processing and microanalysis histories. They were initially embedded in epoxy resin, sectioned, polished and carbon-coated for SEM microanalysis. We collected EMPA (electron microprobe analysis [at the NHM, London on a Cameca SX100]), BSE imaging, EDS (energy dispersive spectrometry) and geochemical (EDX) mapping [using a FEI Quanta 450 ESEM-FEG equipped with EDS Bruker, QUANTAX XFlash detector 6|10 at CISUP] on their exposed interiors. This allowed a more comprehensive analysis of their textures, bulk composition and mineralogy. TAM19B-7 was previously characterised in Suttle et al. (2019a, 2019b) where extensive description of the microanalysis methods can be found. This particle is a hydrated fine-grained micrometeorite with pseudomorphic chondrules and a significant terrestrial weathering overprint. In contrast, TAM20C-345 is a minimally weathered coarse-grained micrometeorite composed of en-

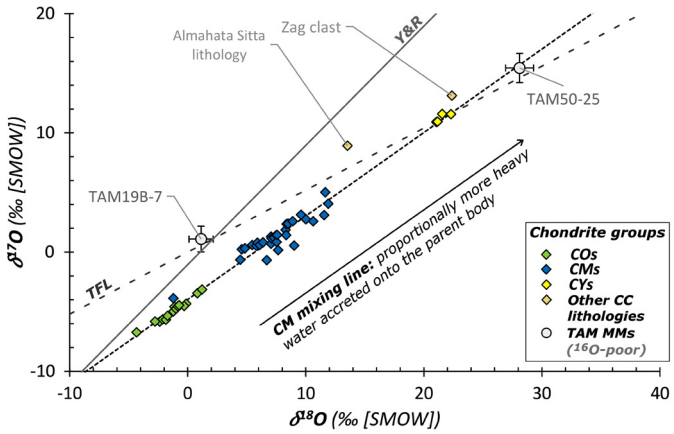

Fig. 5. The CM mixing line in conventional $\delta^{18}O/\delta^{17}O$ isotope space showing CO, CM and CY data from Clayton and Mayeda (1999) with the addition of the (two) ^{16}O-poor TAM micrometeorites presented in this study (TAM19B-7 [weathered] and TAM50-25). For reference we also plot the isotopic compositions of two anomalously heavy carbonaceous chondrite lithologies recently described from the Zag meteorite (Kebukawa et al., 2019) and the Almahata Sitta meteorite (Goodrich et al., 2019) shown in beige. The CO, CM and CY chondrites as well as TAM50-25 share a single isotopic trendline. This potentially represents a genetic relationship and could be explained by the progressive accretion of proportionally more heavy water-ice with the same ^{16}O-poor isotopic composition.

statite phenocrysts and Cr-spinel, embedded in a Ca-rich glass. These particles were plucked from the epoxy resin, soaked in acetone (for 1 week) to remove any remaining resin and then directed for O-isotope measurements, and subsequently treated in an identical manner to the above particles, with the exception that during their O-isotope measurement, the mass spectrometer was also directed to measure for a NF_2 (nitrogen fluoride) peak (with mass 52 [a.m.u]). The presence of which would indicate sample contamination by resin – and imply the presence of NF (with mass 33 [a.m.u]) contamination signal that interferes with the measurement of $(^{16}O+^{17}O)=>O_2$ peak. In both particles (TAM19B7 and TAM20C-345) a NF peak was not observed, suggesting their measurements are unaffected by the resin mounting process.

3. Results

We analysed 14 particles (Figs. 1–3, Table 1) in total, six are coarse-grained, one composite and seven fine-grained (in the classification system of Genge et al., 2008). Average particle diameters vary from 540 µm (TAM50-07) to 2020 µm (TAM19B-7). Chondrules appear in µCT as rounded polymineralic high-density inclusions, while pseudomorphic chondrules are more difficult to detect as only their outlines remain – the high-density anhydrous silicates having been replaced by lower density fine-grained secondary minerals. Based on particle textures, we identify a number of whole chondrules mantled by fine-grained rims (FGR) (e.g. TAM60-01 and TAM50-22) as well as chondrule-bearing particles with either intact (e.g. TAM50-11) or pseudomorphic (e.g. TAM50-25 and TAM50-30) chondrules. Scoriaceous micrometeorites containing a vesicular matrix are also common (e.g. TAM50-01 and TAM50-03). Two particles (TAM50-05 and TAM20C-345) lack clear evidence of chondrules and instead have igneous or metamorphic textures characterised by coarse-grained interlocking crystals.

Isotopic data (Table 1) reveal a wide range of compositions. Ten particles had sufficient mass to produce accurate data (Fig. 4), while the remaining four particles (TAM50-01, TAM50-03, TAM50-07 and TAM50-26) were too small, their isotopic compositions were not well resolved and are therefore not considered further in this study. Of the large mass particles (>0.1 mg) six plot above the TFL (terrestrial fractionation line), defined by the isotopic compositions of Earth's silicate rocks and minerals. In conventional O-

Table 1
Data from 14 giant micrometeorites analysed in this study, showing their masses, textural classifications, O-isotope data, interpreted parent body affinities and their inferred isotopic alteration due to atmospheric entry effects. The following abbreviations are used: coarse-grained micrometeorites (CgMM), fine-grained micrometeorites (FgMM), composite micrometeorite (Comp.), fine-grained rim (FGR) and porphyritic olivine pyroxene chondrule (POP).

ID	*Sample*	*Avg. Size* (μm)	*Type*	*Particle texture from μCT*	*O-isotope data*			*Relative to SMOW (‰)*						*Parent body*		*Atm. Entry shift*	
				Interpretation	*Mass* (μg)	O_2 (μg)	*Yield* (%)	$\delta^{17}O$	$\pm 2\sigma$	$\delta^{18}O$	$\pm 2\sigma$	$\Delta^{17}O$	$\pm 2\sigma$	*Classification*	*Subclass*	*Qualitative*	*Quantified* ($\delta^{18}O$, $\Delta^{17}O$)
1	**TAM60-01**	801	CgMM	Large chondrule + FGR	640	232	36	6.488	*0.668*	10.962	0.876	0.788	*<0.16*	Ordin. Chondr.	L/LL	moderate	+6, -0.5
2	**TAM50-05**	873	CgMM	Interlocking crystalline texture.	382	125	33	4.884	*0.316*	7.405	0.194	1.033	*<0.16*	Ordin. Chondr.	L/LL6	minimal	+2, -0.25
3	**TAM50-09**	744	CgMM	Porphyritic chondrule	256	86	34	6.403	*0.675*	10.760	0.584	0.808	*<0.16*	Ordin. Chondr.	L/LL	moderate	+6, -0.5
4	**TAM50-29**	628	CgMM	Chondrule with distinct grains	221	84	38	5.002	*0.690*	10.370	0.600	-0.390	*<0.16*	Hydr. Carb.	CR	minimal	<+1, +<0.5
5	**TAM20c-345**	1058	CgMM	Igneous texture w/ core + rim	408	171	42	1.590	*0.107*	5.327	0.266	-1.180	*<0.16*	Hydr. Carb.	CR	unaffected	0, 0
6	**TAM50-22**	649	CgMM	POP chondrule. + FGR, weath.	287	63	22	-1.823	*0.886*	0.525	0.814	-2.096	*<0.16*	Hydr. Carb.	CR	unaffected	0, 0
7	**TAM50-11**	762	Comp.	Distinct clasts & Fe-rich regions	305	66	22	4.374	*0.856*	8.101	0.781	0.162	*<0.16*	Enstatite Chondr.	EH	minimal	+2.5, ∼0
8	**TAM50-30**	678	FgMM	Pseudomorphic chondr. + matrix	255	35	14	5.777	*1.141*	13.386	1.091	-1.184	*<0.16*	Hydr. Carb.	CR1	moderate	+5-10, +<0.25
9	**TAM19B-7**	2017	FgMM	Pseudomorphic chondr. + matrix	250	42	17	1.094	*1.080*	1.126	1.024	0.508	*<0.16*	Hydr. Carb.	^{16}O-poor	unknown	*Highly weathered*
10	**TAM50-25**	606	FgMM	Pseudomorphic chondr. + matrix	114	26	23	15.443	*1.227*	28.113	1.184	0.824	*<0.16*	Hydr. Carb.	^{16}O-poor	unknown	Unknown
11	***TAM50-01***	*580*	*FgMM*	*ScMM, no anhydrous silicates*	*89*	*12*	*13*										
12	***TAM50-03***	*612*	*FgMM*	*ScMM, no anhydrous silicates*	*43*	*6*	*14*	*TAM50-01 plots on the TFL while the remaining 3 plot below the TFL.*						*All four are most likely derived from a hydrated carbonaceous chondrite source*		*Low masses & resulting low yields significantly affect the quality of their isotopic data*	
13	***TAM50-07***	*540*	*FgMM*	*Dehydr. Cracks & Fe-rich beads*	*56*	*8*	*14*										
14	***TAM50-26***	*550*	*FgMM*	*Pseudomorphic chondr. + matrix*	*59*	*8*	*14*										

isotopic space [δ^{18}O vs. δ^{17}O] this line has a slope ~0.52, reflecting mass-dependent fractionation processes. The remaining four large micrometeorites plot below the TFL. As a broad generalisation ^{16}O-rich compositions (below the TFL) are associated with carbonaceous chondrite precursors while ^{16}O-poor compositions (above the TFL) generally originate from non-carbonaceous groups (ordinary, enstatite and Rumuruti). However, the CI chondrites, which are a member of the carbonaceous chondrite group plot on and above the TFL (Fig. 4 and Clayton and Mayeda, 1999).

The micrometeorites studied here are related to different chondrite classes. Based on their combined textural and isotopic data eight particles can be matched to specific groups. Two particles plot directly within the measured ranges of their inferred parent body type, while the remaining particles plot relatively close to a single group and their mild offset from a given parent body class can be understood as a product of atmospheric entry alteration (by mass dependent fractionation and mixing with terrestrial oxygen) (Suavet et al., 2010; van Ginneken et al., 2017; Goderis et al., 2020).

4. Discussion

4.1. Particle textures aid isotopic interpretations

A rough estimation of parentage is possible using only textural data from each micrometeorite's unmelted interior (Figs. 1–3). Fine-grained micrometeorites most likely represent samples of chondritic matrix (Genge et al., 2008); they commonly display evidence of parent body aqueous alteration, resulting in the formation of phyllosilicates and other secondary minerals (Taylor et al., 2012; Suttle et al., 2019a). In contrast, coarse-grained micrometeorites mostly sample whole chondrules or chondrule fragments (Genge et al., 2005). However, they may also sample anhydrous precursors such as the CO, CV and CK chondrites, ordinary chondrites (van Ginneken et al., 2012; Cordier et al., 2018) or, in rare cases, differentiated achondritic materials (Gounelle et al., 2009). Composite micrometeorites often comprise both matrix and chondrule material (Genge et al., 2005).

Textures also help constrain the degree of isotopic fractionation away from their pre-atmospheric parent body composition. This occurs due to the combined effects of atmospheric entry (mass-dependent fractionation and mixing with terrestrial oxygen) and contamination by terrestrial weathering caused by mixing with light Antarctic precipitation, which has characteristically low δ^{18}O values (between -30‰ to -55‰, Greenwood et al., 2019). For all the micrometeorites studied here, (except TAM19B-7, Suttle et al., 2019a) terrestrial weathering effects are negligible, specifically because we selected only particles with minimal evidence of terrestrial weathering. The lack of terrestrial alteration is confirmed by their lack of significant encrustation rims, large voids infilled with low density phases (e.g. palagonite, ferrihydrite or calcite), the lack of jarosite veins penetrating particle cores from the perimeter inwards and the lack of etched crystals or glass phases. As such we do not expect weathering to affect the isotopic signatures of these micrometeorites (with the exception of TAM19B-7).

Some particles experienced localised partial melting (notably (TAM50-01 and TAM50-03) as determined by the presence of vesicular matrix, igneous rims or thick well-developed magnetite rims. Moderate shifts in their δ^{18}O towards heavier compositions are expected in these particles as a result of evaporation during atmospheric entry causing mass dependent fractionation. In addition, these particles will have suffered shifts in both their δ^{18}O and Δ^{17}O towards the mesospheric terrestrial oxygen compositions (calculated by Thiemens et al., 1995) reflecting the partial exchange of oxygen with Earth's atmosphere.

4.2. Ordinary chondritic micrometeorites

Three micrometeorites (TAM60-01, TAM50-05 and TAM50-09 – all coarse-grained) are unambiguously associated with the ordinary chondrites. They plot relatively close to the ordinary chondrite field, shifted to higher δ^{18}O values (by approximately +2 to +6‰) and marginally lower (<0.5‰) Δ^{17}O values. These offsets are consistent with expected isotopic entry effects, primarily as a result of exchange with atmospheric oxygen. As a result of their (predicted) isotopic evolution (dashed green lines in Fig. 4) we can confidently assign all three particles to either an L or LL chondrite source body.

Both TAM60-01 and TAM50-09 represent whole chondrules with diameters of 500-800 μm [TAM60-01] and 450-670 μm [TAM50-09], mantled by thick FGRs (<120 μm). These rims partially melted during atmospheric entry resulting in thick melt layers surrounding their unmelted cores. Such features are referred to as igneous rims (Genge, 2006) and in TAM60-01 significant degassing of volatiles appears to have caused the partial detachment of the igneous rim from around the host chondrule, a form of in-flight fragmentation, as described in Suttle et al. (2019b). The average diameter of chondrules in L and LL chondrites are about 700 μm and 900 μm respectively (Weisberg et al., 2006). Thus, chondrule size data, coarse-grained particle textures and isotopic signatures of TAM60-01 and TAM50-09 strongly support an interpretation as ordinary chondrite micrometeorites.

In contrast, TAM50-05 contains no identifiable chondrules and instead its texture resembles an igneous or metamorphic rock, composed of coarse-grained interlocking crystals with interstitial dark and bright phases. This particle therefore appears to be a relatively high-grade metamorphosed chondrite. Since this particle has lost its primary chondrule texture, we can assign a petrologic subtype of (L/LL)6 (Weisberg et al., 2006).

4.3. Hydrated micrometeorites from a CR source

Four micrometeorites analysed in this study have isotopic signatures suggestive of, or clearly associated with, the CR chondrites; they are TAM50-30 (fine-grained), TAM50-22 (composite), TAM50-29 and TAM20C-345 (both coarse-grained). The CR chondrites contain approximately 50-60 vol% chondrules with average diameters of 700 μm (Weisberg et al., 2006). In addition, the extent of aqueous alteration of the CRs varies considerably from minimally altered meteorites such as MET 00426 (a possible CR3.0, Le Guillou and Brearley, 2014) to extensively altered CR1s, such as GRO 95577 (Weisberg and Huber, 2007). This group may therefore contain unaltered, partially replaced or entirely replaced (pseudomorphic) chondrules.

TAM50-22 is a whole chondrule (~280×480 μm) plus FGR (~80-125 μm). This chondrule contains rounded bright regions, most likely Fe-Ni metal droplets (subsequently oxidised) and which are characteristic features of the Mg-rich, type I chondrules. TAM50-29 is similar, with a diameter of 380×620 μm and a granular texture. However, this particle lacks both the internal metal droplets as well as the FGR. Instead a magnetite rim formed during entry (as well as a thin zone of dissolution arising from terrestrial weathering) surround the chondrule margins.

TAM50-30 is a fine-grained matrix-only fragment, which contains minor, small (<20 μm) rounded anhydrous silicate grains. TAM50-30 also contains a single pseudomorphic chondrule with a spherical shape and diameter of ~125 μm (Fig. 1), evidence that this micrometeorite experienced significant aqueous alteration, resulting in the replacement of anhydrous phases. Although 70% of CR chondrites are minimally altered, some intensely altered CR chondrites are known; they contain phyllosilicate fractions up to 0.89 (Howard et al., 2015) and pseudomorphic chondrules (Harju et al., 2014).

While the average chondrule size among the CR chondrites is large (700 μm), small chondrules (~200 μm) and their pseudomorphs are relatively common components of dark inclusions – a form of petrographically distinct unit found within the CR lithology in abundances between 7-25 vol% (Weisberg et al., 1993). These dark inclusions are generally more hydrated than their host chondrites, being dominated by serpentine and saponite, with accessory pyrrhotite laths, pentlandite, magnetite and phosphates (Weisberg and Huber, 2007). They have generally heavier O-isotope compositions than the whole rock CR values, with measured compositions given in Weisberg et al. (1993) at δ^{18}O: 10-13‰ and δ^{17}O: 5.86-6.68‰ (Δ^{17}O: -0.08 to +0.6‰). Thus, TAM50-30 most likely represents a fragment of dark inclusion material from an intensely altered CR chondrite.

In contrast to the above three micrometeorites, the petrographic properties of TAM20C-345 are anomalous. TAM20C-345 has a mineralogy dominated by low-Ca pyroxene (>95%, En_{74-78} Fs_{20} $Wo_{<5}$) with minor Cr-spinel. Both crystalline phases occur within a Ca-bearing silicate glass. Pyroxene minor element contents (FeO [~14.6wt%] vs. MnO [0.35-0.42wt%]/ Cr_2O_3 [0.79-1.1wt%] and CaO [1.9-2.8wt%] vs. Al_2O_3 [2.3-3.5wt%]) fall outside the range of carbonaceous chondrites (CM, CV, CO) and are instead best-matched to the unequilibrated ordinary chondrites (UOCs) (Fig. S2). Pyroxene crystal form skeletal dendritic morphologies and act as a substrate for the nucleation of nano-scale Cr-spinels. This particle has an igneous texture and a bimodal grain size, with a distinct core and rim. The core contains small pyroxene phenocrysts with interstitial poorly-developed Cr-spinel dendrites. It is surrounded by a coarse grained rim composed of Ca-enriched pyroxenes. The rim had variable thickness, contains rounded vesicles and lacks an outer magnetite rim, which is otherwise characteristic of unmelted and scoriaceous micrometeorites (Genge, 2006). TAM20C-345 may therefore record a two-stage cooling history characterised by rapid crystallisation, with the first event representing wholesale melting and quench cooling while the second heating event affected only the particle margin. The outer rim is thus an igneous rim which likely formed during atmospheric entry (Genge, 2006). Assuming TAM20C-345 samples a whole chondrule plus FGR and that this FGR melted completely during entry, the resulting texture can be explained as a product of flash melting and volatile degassing. This scenario is supported by the presence of small vesicles located only within the outer zone of the particle's core. This suggests that surface correlated reduction occurred locally within the chondrule's outer zone during the initial stages of entry heating concurrent with volatile release, principally via the thermal decomposition of carbonaceous material held within the FGR. This would result in the production of recrystalised Fe-enriched pyroxene and Cr-metal at the chondrule margins, as the melted FGR began to cool. However, once the carbon had been lost oxidation by atmospheric oxygen would then take over, converting the earlier produced metal into oxides. A morphologically similar micrometeorite was previously reported by Genge et al. (2005) [Fig. 4C – CP94-100-105] and interpreted as a radiating pyroxene chondrule fragment. Large radiating pyroxene chondrules of similar sizes to TAM20C-345 are found in CR chondrites, but at low abundances (Jones, 2012) and thus, we would expect these materials to be extremely rare among the micrometeorite flux.

4.4. The first documented enstatite chondritic micrometeorite

TAM50-11 (avg. diameter of 762 μm) plots close to the TFL (δ^{18}O=8.10‰ [±0.78‰, 2σ], Δ^{17}O=0.16‰ [±0.16‰, 2σ]) but outside the parent body fields of all chondrite groups. This position represents either a terrestrial particle, an enstatite chondrite affected by minor atmospheric entry effects (mass-dependent fractionation and exchange with terrestrial oxygen) or a CI chondrite (moderately affected terrestrial weathering). Petrographic evidence allows us to differentiate between these possibilities (Fig. 3).

The presence of a magnetite rim and small rounded vesicles demonstrate that this particle is a micrometeorite (with a weakly scoriaceous texture) and implies that the isotopic signature may be mildly affected by entry effects. The internal texture includes faint compact rounded chondrules (marked in Fig. 3), with diameters between 100-250 μm, as well as a relatively high abundance of bright phases, most likely Fe-rich minerals (Fe-metal, Fe-sulfides or Fe-oxides). They occur primarily as irregular-shaped masses that mantle the chondrules (forming armoured chondrules) or as small rounded beads within the larger chondrules (implying type I, first generation Mg-rich chondrules). Because the chondrule outlines in TAM50-11 are poorly resolved this implies the particle was subject to thermal metamorphism and is therefore an equilibrated meteorite with a petrologic subtype higher than 3, most likely a subtype 4 which is defined as: "*some chondrules can be discerned, few sharp edges*" (Weisberg et al., 2006). Since CI chondrites lack chondrules, TAM50-11 cannot be a member of this group. Instead, this micrometeorite is consistent with a high-iron enstatite chondrite (EH) whose average chondrule size (~200 μm) and relative chondrule abundance (between 60-80vol%, Weisberg et al., 2006) closely match the observed textures in TAM50-11. Furthermore, the enstatite chondrites have highly reduced mineralogy which commonly contains zoned, porphyritic and radiating pyroxene chondrules that may have armoured sulphide mantles and large sulphide masses (Weisberg and Kimura, 2012). Thus, TAM50-11 demonstrates clear affinities to the enstatite chondrites and is therefore interpreted as the first documented enstatite chondritic micrometeorite.

4.5. The anomalous ^{16}O-poor micrometeorites

Two of the micrometeorites studied here (TAM19B-7, TAM50-25) combine aqueously altered hydrated carbonaceous chondrite textures with O-isotopic signatures that plot above the TFL (Fig. 4 and Fig. 5). For TAM19B-7, the primary isotopic composition has been shifted to lower δ^{18}O values as a result of mixing and exchange with Antarctic precipitation (Alexander et al., 2018; Greenwood et al., 2019). Thus, the reconstructed unweathered isotopic composition of TAM19B-7 lies somewhere at higher Δ^{17}O and δ^{18}O values (Fig. 4 dashed red line). These two ^{16}O-poor micrometeorites are noteworthy because most carbonaceous chondrites, except the CI chondrites and the newly defined CY chondrites (King et al., 2019) plot below the TFL. Recently, additional heavy ^{16}O-poor isotopic compositions have been reported from other carbonaceous materials. An organic-rich dark clast in the Zag meteorite (a H ordinary chondrite) was found with a composition of δ^{17}O: +13.13‰, δ^{18}O: +22.38‰, Δ^{17}O: +1.49 ‰ (Kebukawa et al., 2019), while chondritic lithologies within the Almahata Sitta meteorite (an anomalous polymict breccia) have measured compositions of δ^{17}O: +8.93‰, δ^{18}O: +13.53‰, Δ^{17}O: +1.89‰ (Goodrich et al., 2019). Both these lithologies are isotopically distinct from the measured compositions of TAM50-25 and TAM19B-7 (Figs. 4 & 5) suggesting that they are not related. Instead they further demonstrate that a variety of ^{16}O-poor carbonaceous chondrite compositions (plotting above the TFL) exist but have yet to be fully characterised.

Isotopically heavy micrometeorites are of particular interest because previous studies on giant cosmic spherules (>500 μm) identified similar ^{16}O-poor compositions (Fig. 4). The ^{16}O-poor micrometeorites studied here (TAM50-25 and TAM19B-7) are therefore potentially derived from the same population (Yada et al., 2005; Suavet et al., 2010; van Ginneken et al., 2017; Goderis et al., 2020). The ^{16}O-poor cosmic spherules previously reported by Suavet et al. (2010) were termed "Group 4" because among a population of

33 particles only four distinct clusters were identified, relating to the CV/CO/CM chondrites (group 1), the CR chondrites (group 2), the ordinary chondrites (group 3) and an enigmatic ^{16}O-poor class (Group 4). This final group appears to be otherwise unsampled by known meteorite groups and thus new to the field of meteoritics and planetary science (Suavet et al., 2010).

The Group 4 micrometeorites in Suavet et al. (2010) plot above the TFL, with similar Δ^{17}O values to the ordinary chondrites ($\sim$+1-2‰) but notably higher δ^{18}O values (>40‰). Based on relatively small statistical populations they represent >10% and $\ll$30% of the micrometeorite flux, at size fractions above 500 μm (Suavet et al., 2010; van Ginneken et al., 2017). However, the petrographic properties of the Group 4 micrometeorite are unknown. This is because all previous isotope studies which identified and analysed members of this class were performed on melted cosmic spherules – particles which had lost their pre-atmospheric parent body texture and mineralogy owing to complete melting during atmospheric entry (Genge et al., 2008). As a result, analysis of the Group 4 spherules could not provide the necessary petrographic information to adequately characterize their parent body source.

New perspectives from this study suggest that the ^{16}O-poor Group 4 micrometeorites are most likely a type of hydrated fine-grained micrometeorite associated with the aqueously altered carbonaceous chondrites. Micro-CT slices through TAM50-25 reveal a dark scoriaceous matrix containing dehydration cracks and rounded vesicles, formed during atmospheric entry. These textural features are diagnostic of hydrated micrometeorites (Genge et al., 2008; Suttle et al., 2019a, 2019b). Furthermore, TAM50-25 contains a single pseudomorphic chondrule (Fig. 1, 215-250 μm diameter), as well as minor relict anhydrous silicate crystals with rounded morphologies. Likewise, TAM19B-7 (Fig. 2 and described in Suttle et al. (2019a)) is an exceptionally large (>2000 μm avg. diameter) hydrated fine-grained micrometeorite containing at least four pseudomorphic chondrules with similar sizes (between 140-180 μm). They are mantled by variable thickness FGRs (all <100 μm in thickness). Both particles are intensely altered, as evidenced by their high phyllosilicate fractions (0.97 in TAM19B-7) and minimal surviving primary anhydrous silicate contents. In addition, TAM19B-7 was previously found to contain a pervasive low-grade petrofabric, identified by the presence of aligned phyllosilicates (Suttle et al., 2019a) and suggestive of shock processing – potentially by successive low-intensity impacts (Lindgren et al., 2015).

4.6. ^{16}O-poor micrometeorites and their relationship to the CY chondrites

Recently, King et al. (2019) reviewed evidence for the existence of an additional subgroup of hydrated carbonaceous chondrites, termed the CY chondrites; originally proposed by Ikeda (1992). This class is composed of six Antarctic meteorites (King et al., 2019). Most members are currently classified as ungrouped C1 or C2 chondrites in the Meteoritical Bulletin (2020). They include Yamato (Y)-82162 [C1/2-ung], Y-86720 [C2-ung], Belgica (B)-7904 [C2-ung], Y-86789 [C2-ung], Y-86029 [CI1] and Y-980115 [CI1]. However, additional CY meteorites are likely to exist, with the following probable candidates identified: Dho 225 [CM-an] and Dho 735 [CM2] (Ivanova et al., 2010) and Dho 1988 [C2-ung] and Dho 2066 [C-ung] (King et al., 2019).

The CY chondrites have a distinct alteration history defined by an initial period of intense aqueous alteration, resulting in the secondary replacement of almost the entire anhydrous silicate content and thus the formation of pseudomorphic chondrules. This was followed by, or transitioned into, an episode of thermal metamorphism at temperatures >500°C (Ikeda, 1992; King et al., 2019). The resulting mineral assemblage is dominated by dehydrated phyllosilicates. Other characteristic features are Na-bearing saponite, anomalously high sulphide contents (15-20vol%, Ikeda, 1992; King et al., 2015), Fe-bearing periclase and in some members a range of magnetite morphologies (plaquettes, framboidal and spherulitic) (Ikeda, 1992; King et al., 2019).

The CY chondrites are united by a distinct O-isotopic signature, originally identified by Clayton and Mayeda (1999), which is both heavier than all other carbonaceous chondrites (Fig. 5) and close to the intersection of the TFL and CM mixing line, with isotopic ratios of approximately δ^{18}O>22‰ and Δ^{17}O$\geq$0‰. The CY chondrites are thus the closest parent body in isotopic space to the ^{16}O-poor micrometeorites described here and could therefore represent either the same or a related parent body. Although their petrographic properties and alteration histories are similar, they are not identical. For example, the size range of intact and pseudomorphic chondrules in CY chondrites, although poorly constrained, appears to be significantly larger than those identified in TAM50-25 and TAM19B-7. Chondrules in the CY chondrite B-7904 range from 500-2000 μm in size (Bischoff and Metzler, 1991), while in Y-86789 they range from 600-750 μm in diameter (Matsuoka et al., 1996). Likewise, the CY chondrites appear to have notably high sulphide contents (10-30 vol%, King et al., 2019) and a more diverse mineralogy. The ^{16}O-poor micrometeorites analysed here do not contain evidence of abundant sulphide, although this could have been lost during atmospheric entry. At present, detailed comparison of the two population's petrographic properties is not currently possible due to the lack of a representative sampling of the new ^{16}O-poor micrometeorites.

4.7. The effects of thermal metamorphism

Alternatively, the ^{16}O-poor micrometeorites may be unrelated to the CY chondrites and instead represent fragments of thermally metamorphosed CM chondrite. Experimental studies heating CM chondrites have produced heavier bulk O-isotope compositions in the dehydrated reaction products with δ^{18}O enrichments between +5‰ to +10‰ (Clayton and Mayeda, 1999; Ivanova et al., 2010). This effect occurs due to a preferential loss of isotopically light (^{16}O-rich) oxygen released during phyllosilicate dehydration (Clayton and Mayeda, 1999; Ivanova et al., 2010). These experiments imply that the heavy O-isotope compositions of both the CY chondrites and the ^{16}O-poor micrometeorites could be, at least in part, due to thermal metamorphism. However, when Nakamura (2005) compared 21 carbonaceous chondrites (both unheated and thermally metamorphosed samples) they found no clear relationship between bulk O-isotope composition and the degree of thermal metamorphism suggesting that metamorphic overprints play a relatively modest role in controlling the final bulk O-isotope composition of chondrites. Instead their formation mechanisms are more significant.

4.8. The accretion of heavy water

In oxygen isotope space (δ^{18}O/δ^{17}O) the CO, CM and CY chondrites plot along a single trendline with a slope of $\sim$0.7 (and a δ^{17}O intercept of -4.23‰, Clayton and Mayeda, 1999). This is referred to as the *CM mixing line* (Fig. 5 and Clayton and Mayeda, 1999; Greenwood et al., 2019). One of the ^{16}O-poor micrometeorites studied here (TAM50-25) also plots on this line (Fig. 5). This line represents mixing between two isotopically distinct end-member components: a solar-like ^{16}O-rich silicate source and a ^{16}O-poor "*aqueous reservoir*" (Clayton and Mayeda, 1999). Meteorites that plot with heavier bulk O-isotope compositions most likely reflect bodies which accreted proportionally more heavy water-ice. The anhydrous CO chondrites have the lightest bulk O-isotope compositions, while the hydrated CM chondrites have heavier compositions (Fig. 5). Furthermore, the CM2 chondrites

display a weak correlation between their bulk O-isotope composition and the extent of aqueous alteration (Fig. 8 in Rubin et al., 2007; Howard et al., 2010; Franchi et al., 2019). However, this relationship does not hold true for the more intensely aqueously altered CM1 chondrites (Franchi et al., 2019).

Because water-ice was the main carrier phase of heavy oxygen (Clayton and Mayeda, 1999; Chaumard et al., 2018), the amount of water initially accreted onto the parent body should control, at least partially, the final extent of aqueous alteration. However, other factors such as duration, temperature and whether aqueous alteration operated as an open or closed system could have affected the extent of aqueous alteration (Ivanova et al., 2010; Schrader and Davidson, 2017). These processes may have resulted in a decoupling of accreted water content from the final bulk O-isotope composition (as may be the case for the CM1s [Franchi et al., 2019]).

The CY chondrites and the ^{16}O-poor micrometeorites are the heaviest representatives of the CM mixing line. Their position implies that they accreted at least as much water as the CM chondrites, potentially more. In addition, a later episode of thermal metamorphism would have played a role in further increasing the bulk O-isotope composition of the dehydrated CY chondrites and perhaps also affected the ^{16}O-poor micrometeorites (section 4.7). In either scenario, their presence on the CM mixing line implies a close relationship, and formation by fundamentally the same mechanisms. These different chondrite groups could reflect material derived from a single body (Franchi et al., 2019), formed within the same region of the protoplanetary disk but at different times (e.g. Chaumard et al., 2018) or close asteroidal neighbours (e.g. Schrader and Davidson, 2017).

5. Implications for the flux of extraterrestrial material

Most micrometeorites in this study can be directly matched to established chondrite groups. However, the presence of TAM50-25, whose isotopic signature is uniquely heavy (δ^{18}O: 28.11‰ and Δ^{17}O: 0.82‰) and sufficiently distinct from all known chondrite groups demonstrates that some micrometeorites originate from new and previously unknown parent bodies. TAM50-25 is most likely a member of the Group 4 population previously described by Yada et al. (2005), Suavet et al. (2010) and others. This population represents between 10-30% of the micrometeorite flux at large size fractions (Suavet et al., 2010; van Ginneken et al., 2017). Evidence from TAM50-25 shows that the Group 4 parent body is intensely aqueously altered and potentially lacks anhydrous chondrule material, similar to the CI chondrites. Currently, there are <10 officially recognised CI chondrites (The Meteoritical Bulletin, 2020). Their rarity may be a product of destruction during atmospheric entry combined with rapid weathering rates. Conversely, hydrated micrometeorites preferentially survive atmospheric entry. Their high water contents act as heat sinks, generating strong thermal gradients that allow the core to survive relatively unheated (Genge, 2006; Suttle et al., 2019b). Micrometeorites offer a complementary perspective to that obtained from research on larger meteorite collections, originating from parent bodies that would otherwise remain unsampled.

6. Conclusions

This is the first study systematically employ a combined textural and isotopic approach to the parent body identification of giant (>400 µm) unmelted and scoriaceous micrometeorites. We paired particle textures against parent body groups (defined by O-isotope data). Most particles were related to either ordinary chondrites of the L or LL subgroups (30%) or CR chondrites (40%). However, we also identified the first enstatite chondrite (EH4) micrometeorite. In addition, we identified two ^{16}O-poor micrometeorites (TAM19B-7 and TAM50-25) interpreted as unmelted representatives of the previously defined Group 4 population (Suavet et al., 2010). Pre-characterisation demonstrated that these ^{16}O-poor micrometeorites are hydrated fine-grained particles with petrographic features similar to the CM1/CR1 chondrites. TAM50-25 has an O-isotopic signature which plots on the CM mixing line at heavier O-isotope compositions than all previously reported meteorite samples. This position implies a close relationship with (and potentially a genetic link to) the CO, CM and CY chondrites. In addition, its isotopic composition attests to the accretion of significant quantities of heavy ^{16}O-poor water (at least as much as the CM chondrites, but potentially more). The discovery of these micrometeorites and other ^{16}O-poor materials (e.g. Zag meteorite clast and Almahata Sitta lithologies) reveal hidden diversity of hydrated carbonaceous chondrite parent bodies.

This study demonstrates the importance of studying micrometeorites, especially giant representatives as they are a complementary branch of meteoritics whose extraterrestrial materials are vital to furthering our understanding of the asteroid belt's diversity and the solar system's evolution.

Declaration of competing interest

The authors declare that they have no known competing financial interests or personal relationships that could have appeared to influence the work reported in this paper.

Acknowledgements

Micro-CT data collected at the SOLEIL Synchrotron was funded through proposal no. 20180438. O-isotope data collection was funded through a Europlanet2020 transnational access grant (18-EPN4-060) – itself funded by the European Union's Horizon 2020 research and innovation programme under grant agreement No. 654208. Funding for micrometeorite research at the Universities of Pisa and Napoli is facilitated through two Italian research grants MIUR: PNRA16_00029 [Programma Nazionale delle Ricerche in Antartide – CUP I52F17001050005] and PRIN2015_20158W4JZ7 [CUP I52F15000310001 for the "Meteoriti Antartiche"]. We also wish to thank the Italian Space Agency (ASI, Italy) on contract no. I/024/12/2. Funding for research on water-rich asteroids is supported by the UK's Science and Technology Facilities Council (STFC) grant no. ST/R000727/1. Planetary science research studies at the Open University are supported by a Consolidated Grant from the UK Science and Technology Facilities Council (STFC), Grant number: ST/P000657/1. We thank M. Genge for useful discussions on the interpretation of TAM20C-345, two anonymous reviewers for their helpful comments and insights and to the associate editor William B. McKinnon for handling the manuscript during the review process.

Appendix A. Supplementary material

Supplementary material related to this article can be found online at https://doi.org/10.1016/j.epsl.2020.116444.

References

Alexander, C.M.O'D., Greenwood, R.C., Bowden, R., Gibson, J.M., Howard, K.T., Franchi, I.A., 2018. A mutli-technique search for the most primitive CO chondrites. Geochim. Cosmochim. Acta 221, 406–420. https://doi.org/10.1016/j.gca.2017.04.021.

Battandier, M., Bonal, L., Quirico, E., Beck, P., Engrand, C., Duprat, J., Dartois, E., 2018. Characterization of the organic matter and hydration state of Antarctic micrometeorites: a reservoir distinct from carbonaceous chondrites. Icarus 306, 74–93. https://doi.org/10.1016/j.icarus.2018.02.002.

Bischoff, A., Metzler, K., 1991. Mineralogy and petrography of the anomalous carbonaceous chondrites Yamato-86720, Yamato-82162, and Belgica-7904. Antarct. Meteor. Res. 4, 226–246.

Brearley, A.J., Jones, R.H., 1998. Chondritic meteorites. In: Papike, J.J. (Ed.), Planetary Materials: Mineralogical Society of America Reviews in Mineralogy, vol. 36, pp. 120–518.

Chaumard, N., Defouilloy, C., Kita, N.T., 2018. Oxygen isotope systematics of chondrules in the Murchison CM2 chondrite and implications for the CO-CM relationship. Geochim. Cosmochim. Acta 228, 220–242. https://doi.org/10.1016/j.gca.2018.02.040.

Clayton, R.N., Mayeda, T.K., 1999. Oxygen isotope studies of carbonaceous chondrites. Geochim. Cosmochim. Acta 63, 2089–2104. https://doi.org/10.1016/S0016-7037(99)00090-3.

Cordier, C., Folco, L., 2014. Oxygen isotopes in cosmic spherules and the composition of the near-Earth interplanetary dust complex. Geochim. Cosmochim. Acta 146, 18–26. https://doi.org/10.1016/j.gca.2014.09.038.

Cordier, C., Baecker, B., Ott, U., Folco, L., Trieloff, M., 2018. A new type of oxidized and pre-irradiated micrometeorite. Geochim. Cosmochim. Acta 233, 135–158.

Engrand, C., Maurette, M., 1998. Carbonaceous micrometeorites from Antarctica. Meteorit. Planet. Sci. 33, 565–580. https://doi.org/10.1111/j.1945-5100.1998.tb01665.x.

Engrand, C., McKeegan, K.D., Leshin, L.A., Herzog, G.F., Schnabel, C., Nyquist, L.E., Brownlee, D.E., 2005. Isotopic compositions of oxygen, iron, chromium, and nickel in cosmic spherules: toward a better comprehension of atmospheric entry heating effects. Geochim. Cosmochim. Acta 69, 5365–5385. https://doi.org/10.1016/j.gca.2005.07.002.

Folco, L., Cordier, C., 2015. Micrometeorites. https://doi.org/10.1180/EMU-notes15.9.

Franchi, I.A., Greenwood, R.C., Howard, K.T., King, A.J., Lee, M.R., Anand, M., Findlay, R., 2019. Oxygen isotope variation of CM and related chondrites: multiple parent bodies or a single heterogeneous source? In: 82nd Annual Meeting of the Meteoritical Society. 7-12 July (Abstr.#6482).

Genge, M.J., 2006. Igneous rims on micrometeorites. Geochim. Cosmochim. Acta 70, 2603–2621. https://doi.org/10.1016/j.gca.2006.02.005.

Genge, M.J., Gileski, A., Grady, M.M., 2005. Chondrules in Antarctic micrometeorites. Meteorit. Planet. Sci. 40, 225–238. https://doi.org/10.1111/j.1945-5100.2005.tb00377.x.

Genge, M.J., Engrand, C., Gounelle, M., Taylor, S., 2008. The classification of micrometeorites. Meteorit. Planet. Sci. 43, 497–515. https://doi.org/10.1111/j.1945-5100.2008.tb00668.x.

Goderis, S., Soens, B., Huber, M.S., McKibbin, S., Van Ginneken, M., Van Maldeghem, F., Debaille, V., Greenwood, R.C., Franchi, I.A., Cnudde, V., Van Malderen, S., 2020. Cosmic spherules from Widerøefjellet, Sør Rondane Mountains (East Antarctica). Geochim. Cosmochim. Acta 270, 112–143. https://doi.org/10.1016/j.gca.2019.11.016.

Goodrich, C.A., Zolensky, M.E., Fioretti, A.M., Shaddad, M.H., Downes, H., Hiroi, T., Kohl, I., Young, E.D., Kita, N.T., Hamilton, V.E., Riebe, M.E., 2019. The first samples from Almahata Sitta showing contacts between ureilitic and chondritic lithologies: implications for the structure and composition of asteroid 2008 TC 3. Meteorit. Planet. Sci. 54, 2769–2813. https://doi.org/10.1111/maps.13390.

Gounelle, M., Engrand, C., Maurette, M., Kurat, G., McKeegan, K.D., Brandstatter, F., 2005. Small Antarctic micrometeorites: a mineralogical and in situ oxygen isotope study. Meteorit. Planet. Sci. 40, 917–932. https://doi.org/10.1111/j.1945-5100.2005.tb00163.x.

Gounelle, M., Chaussidon, M., Morbidelli, A., Barrat, J.A., Engrand, C., Zolensky, M.E., McKeegan, K.D., 2009. A unique basaltic micrometeorite expands the inventory of solar system planetary crusts. Proc. Natl. Acad. Sci. USA 106, 6904–6909. https://doi.org/10.1073/pnas.0900328106.

Greenwood, R.C., Burbine, T.H., Miller, M.F., Franchi, I.A., 2017. Melting and differentiation of early-formed asteroids: the perspective from high precision oxygen isotope studies. Chem. Erde 77, 1–43. https://doi.org/10.1016/j.chemer.2016.09.005.

Greenwood, R.C., Howard, K.T., King, A.J., Lee, M.R., Burbine, T.H., Franchi, I.A., Anand, M., Findlay, R., Gibson, M., 2019. Oxygen isotope evidence for multiple CM parent bodies: what will we learn from the Hayabusa2 and OSIRIS-REx sample return missions? In: Lunar and Planetary Science Conference, vol. 50 (Abstract #3191).

Harju, E.R., Rubin, A.E., Ahn, I., Choi, B.G., Ziegler, K., Wasson, J.T., 2014. Progressive aqueous alteration of CR carbonaceous chondrites. Geochim. Cosmochim. Acta 139, 267–292. https://doi.org/10.1016/j.gca.2014.04.048.

Howard, K.T., Benedix, G.K., Bland, P.A., Greenwood, R.C., Franchi, I., Cressy, G., 2010. Correlated modal mineralogy, aqueous alteration and oxygen isotope composition of CM chondrites. In: 41st Lunar and Planetary Science Conference, pp. 1–5 (Abstr.#1595).

Howard, K.T., Alexander, C.O.D., Schrader, D.L., Dyl, K.A., 2015. Classification of hydrous meteorites (CR, CM and C2 ungrouped) by phyllosilicate fraction: PSD-XRD modal mineralogy and planetesimal environments. Geochim. Cosmochim. Acta 149, 206–222. https://doi.org/10.1016/j.gca.2014.10.025.

Ikeda, Y., 1992. An overview of the research consortium, "Antarctic carbonaceous chondrites with CI affinities, Yamato-86720, Yamato-82162, and Belgica-7904". Antarct. Meteor. Res. 5, 49–73.

Ivanova, M.A., Lorenz, C.A., Nazarov, M.A., Brandstaetter, F., Franchi, I.A., Moroz, L.V., Clayton, R.N., Bychkov, A.Y., 2010. Dhofar 225 and Dhofar 735: Relationship to CM2 chondrites and metamorphosed carbonaceous chondrites Belgica-7904 and Yamato-86720. Meteorit. Planet. Sci. 45, 1108–1123. https://doi.org/10.1111/j.1945-5100.2010.01064.x.

Jones, R.H., 2012. Petrographic constraints on the diversity of chondrule reservoirs in the protoplanetary disk. Meteorit. Planet. Sci. 47, 1176–1190. https://doi.org/10.1111/j.1945-5100.2011.01327.x.

Kebukawa, Y., Ito, M., Zolensky, M.E., Greenwood, R.C., Rahman, Z., Suga, H., Nakato, A., Chan, Q.H., Fries, M., Takeichi, Y., Takahashi, Y., 2019. A novel organic-rich meteoritic clast from the outer solar system. Sci. Rep. 9, 1–8. https://doi.org/10.1038/s41598-019-39357-1.

King, A.J., Schofield, P.F., Howard, K.T., Russell, S.S., 2015. Modal mineralogy of CI and CI-like chondrites by X-ray diffraction. Geochim. Cosmochim. Acta 165, 148–160. https://doi.org/10.1016/j.gca.2015.05.038.

King, A.J., Bates, H.C., Krietsch, D., Busemann, H., Clay, P.L., Schofield, P.F., Russell, S.S., 2019. The Yamato-type (CY) carbonaceous chondrite group: analogues for the surface of asteroid Ryugu? Chem. Erde. CHEMER_2019_70.

Le Guillou, C., Brearley, A., 2014. Relationships between organics, water and early stages of aqueous alteration in the pristine CR3.0 chondrite MET 00426. Geochim. Cosmochim. Acta 131, 344–367. https://doi.org/10.1016/j.gca.2013.10.024.

Lindgren, P., Hanna, R.D., Dobson, K.J., Tomkinson, T., Lee, M.R., 2015. The paradox between low shock-stage and evidence for compaction in CM carbonaceous chondrites explained by multiple low-intensity impacts. Geochim. Cosmochim. Acta 148, 159–178. https://doi.org/10.1016/j.gca.2014.09.014.

Matsuoka, K., Nakamura, T., Nakamuta, Y., Takaoka, N., 1996. Yamato-86789: a heated CM-like carbonaceous chondrite. Antarct. Meteor. Res. 9, 20–36.

Miller, M.F., Franchi, I.A., Sexton, A.S., Pillinger, C.T., 1999. High precision δ17O isotope measurements of oxygen from silicates and other oxides: method and applications. Rapid Commun. Mass Spectrom. 13, 1211–1217. https://doi.org/10.1002/(SICI)1097-0231(19990715)13:13<1211::AID-RCM576>3.0.CO;2-M.

Nakamura, T., 2005. Post-hydration thermal metamorphism of carbonaceous chondrites. J. Mineral. Petrol. Sci. 100, 260–272. https://doi.org/10.2465/jmps.100.260.

Prasad, M.S., Rudraswami, N.G., de Araujo, A.A., Khedekar, V.D., 2018. Characterisation, sources and flux of unmelted micrometeorites on Earth during the last ~50,000 years. Sci. Rep. 8, 8887. https://doi.org/10.1038/s41598-018-27158-x.

Rochette, P., Folco, L., Suavet, C., Van Ginneken, M., Gattacceca, J., Perchiazzi, N., Braucher, R., Harvey, R.P., 2008. Micrometeorites from the transantarctic mountains. Proc. Natl. Acad. Sci. 105, 18206–18211. https://doi.org/10.1073/pnas.0806049105.

Rubin, A.E., Trigo-Rodríguez, J.M., Huber, H., Wasson, J.T., 2007. Progressive aqueous alteration of CM carbonaceous chondrites. Geochim. Cosmochim. Acta 71, 2361–2382. https://doi.org/10.1016/j.gca.2007.02.008.

Sakamoto, K., Nakamura, T., Noguchi, T., Tsuchiyama, A., 2010. A new variant of saponite-rich micrometeorites recovered from recent Antarctic snowfall. Meteorit. Planet. Sci. 45, 220–237. https://doi.org/10.1111/j.1945-5100.2010.01019.x.

Schrader, D.L., Davidson, J., 2017. CM and CO chondrites: a common parent body or asteroidal neighbors? Insights from chondrule silicates. Geochim. Cosmochim. Acta 214, 157–171. https://doi.org/10.1016/j.gca.2017.07.031.

Starkey, N.A., Jackson, C.R.M., Greenwood, R.C., Parman, S., Franchi, I.A., Jackson, M., Fitton, J.G., Stuart, F.M., Kurz, M., Larsen, L.M., 2016. Triple oxygen isotopic composition of the high ^{3}He/^{4}He mantle. Geochim. Cosmochim. Acta 176, 227–238. https://doi.org/10.1016/j.gca.2015.12.027.

Suavet, C., Alexandre, A., Franchi, I.A., Gattacceca, J., Sonzogni, C., Greenwood, R.C., Folco, L., Rochette, P., 2010. Identification of the parent bodies of micrometeorites with high-precision oxygen isotope ratios. Earth Planet. Sci. Lett. 293, 313–320. https://doi.org/10.1016/j.epsl.2010.02.046.

Suavet, C., Rochette, P., Kars, M., Gattacceca, J., Folco, L., Harvey, R.P., 2009. Statistical properties of the Transantarctic Mountains (TAM) micrometeorite collection. Polar Sci. 3, 100–109. https://doi.org/10.1016/j.polar.2009.06.003.

Suttle, M.D., Folco, L., 2020. The extraterrestrial dust flux: size distribution and mass contribution estimates inferred from the transantarctic mountains (TAM) micrometeorite collection. J. Geophys. Res., Planets 125. https://doi.org/10.1029/2019JE006241.

Suttle, M.D., Folco, L., Genge, M.J., Russell, S.S., Najorka, J., van Ginneken, M., 2019a. Intense aqueous alteration on C-type asteroids: perspectives from giant fine-grained micrometeorites. Geochim. Cosmochim. Acta 245, 352–373. https://doi.org/10.1016/j.gca.2018.11.019.

Suttle, M.D., Genge, M.J., Folco, L., Van Ginneken, M., Lin, Q., Russell, S.S., Najorka, J., 2019b. The atmospheric entry of fine-grained micrometeorites: the role of volatile gases in heating and fragmentation. Meteorit. Planet. Sci. 54, 503–520. https://doi.org/10.1111/maps.13220.

Taylor, S., Matrajt, G., Guan, Y., 2012. Fine-grained precursors dominate the micrometeorite flux. Meteorit. Planet. Sci. 47, 550–564. https://doi.org/10.1111/j.1945-5100.2011.01292.x.

The Meteoritical Bulletin, 2020. Accessed on 22/06/2020 and available at: https://www.lpi.usra.edu/meteor/metbull.php.

Thiemens, M.H., Jackson, T., Zipf, E.C., Erdman, P.W., van Egmond, C., 1995. Carbon dioxide and oxygen isotope anomalies in the mesosphere and stratosphere. Science 270, 969–972. https://doi.org/10.1126/science.270.5238.969.

van Ginneken, M., Folco, L., Cordier, C., Rochette, P., 2012. Chondritic micrometeorites from the transantarctic mountains. Meteorit. Planet. Sci. 47, 228–247. https://doi.org/10.1111/j.1945-5100.2011.01322.x.

van Ginneken, M., Genge, M.J., Folco, L., Harvey, R.P., 2016. The weathering of micrometeorites from the transantarctic mountains. Geochim. Cosmochim. Acta 179, 1–31. https://doi.org/10.1016/j.gca.2015.11.045.

van Ginneken, M., Gattacceca, J., Rochette, P., Sonzogni, C., Alexandre, A., Vidal, V., Genge, M.J., 2017. The parent body controls on cosmic spherule texture: evidence from the oxygen isotopic compositions of large micrometeorites. Geochim. Cosmochim. Acta 212, 196–210. https://doi.org/10.1016/j.gca.2017.05.008.

Weisberg, M.K., Huber, H., 2007. The GRO 95577 CR1 chondrite and hydration of the CR parent body. Meteorit. Planet. Sci. 42, 1495–1503. https://doi.org/10.1111/j.1945-5100.2007.tb00587.x.

Weisberg, M.K., Kimura, M., 2012. The unequilibrated enstatite chondrites. Chem. Erde 72, 101–115. https://doi.org/10.1016/j.chemer.2012.04.003.

Weisberg, M.K., Prinz, M., Clayton, R.N., Mayeda, T.K., 1993. The CR (Renazzo-type) carbonaceous chondrite group and its implications. Geochim. Cosmochim. Acta 57, 1567–1586. https://doi.org/10.1016/0016-7037(93)90013-M.

Weisberg, M.K., McCoy, T.J., Krot, A.N., 2006. Systematics and evaluation of meteorite classification. In: Meteorites and the Early Solar System II.

Yada, T., Nakamura, T., Noguchi, T., Matsumoto, N., Kusakabe, M., Hiyagon, H., Ushikubo, T., Sugiura, N., Kojima, H., Takaoka, N., 2005. Oxygen isotopic and chemical compositions of cosmic spherules collected from the Antarctic ice sheet: implications for their precursor materials. Geochim. Cosmochim. Acta 69, 5789–5804. https://doi.org/10.1016/j.gca.2005.08.002.